A novel radioguided surgery technique exploiting β^- decays

E. Solfaroli Camillocci[a], G. Baroni[b], F. Bellini[c,d], V. Bocci[d], F. Collamati[c,d], M. Cremonesi[e], E. De Lucia[j], P. Ferroli[f], S. Fiore[d,g], C. M. Grana[e], M. Marafini[h,d], I. Mattei[i,j], S. Morganti[d], G. Paganelli[m], V. Patera[k,d], L. Piersanti[k,j], L. Recchia[d], A. Russomando[a,c,d], M. Schiariti[f], A. Sarti[k,j], A. Sciubba[k,d], C. Voena[d], R. Faccini[c,d]

[a] *Center for Life Nano Science@Sapienza, Istituto Italiano di Tecnologia, Roma, Italy.*
[b] *Dip. Elettronica, Informazione e Bioingegneria, Politecnico di Milano, Italy;*
[c] *Dip. Fisica, Sapienza Univ. di Roma, Roma, Italy;*
[d] *INFN Sezione di Roma, Roma, Italy;*
[e] *Istituto Europeo di Oncologia, Milano, Italy;*
[f] *Fondazione Istituto Neurologico Carlo Besta, Milano, Italy;*
[g] *ENEA UTTMAT-IRR, Casaccia R.C., Roma, Italy;*
[h] *Museo Storico della Fisica e Centro Studi e Ricerche 'E. Fermi', Roma, Italy;*
[i] *Dipartimento di Fisica, Università Roma Tre, Roma, Italy;*
[j] *Laboratori Nazionali di Frascati dell'INFN, Frascati, Italy;*
[k] *Dip. Scienze di Base e Applicate per l'Ingegneria, Sapienza Univ. di Roma, Roma, Italy.*
[m] *Department of Nuclear Medicine and Radiometabolic Unit, Istituto Scientifico Romagnolo per lo Studio e la Cura dei Tumori, IRST-IRCCS, Meldola, Italy*

February 10, 2014

Supplementary Information

Probe test in laboratory

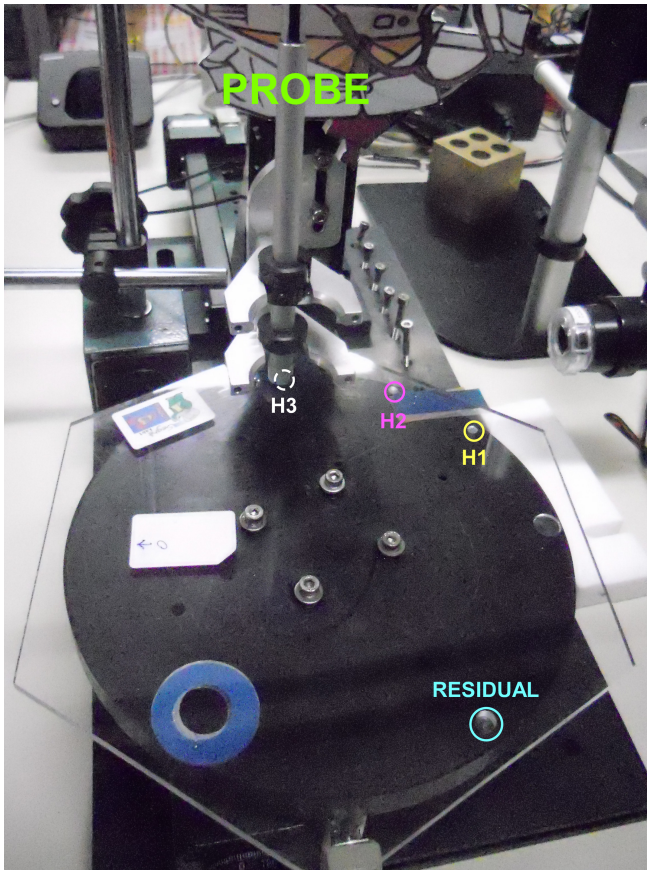

Supplementary Figure S1: **Experimental set-up.** The probe and the automated disk with phantoms for the ^{90}Y tests.

Supplementary Discussion on the probe test results. We observed that the probe prototype is able to detect samples of millimetric dimensions and different topologies in the whole activity concentration range suitable for diagnostic investigation (5-22 kBq/ml). The counts-per-second (cps) measured by the probe on any phantom decrease, as expected, with the ^{90}Y activity according to the radionuclide decay law, as shown in Supplementary Fig. S2 for the RESIDUAL phantom.

To test the detection efficiency of the probe and its sensitivity to different phantom topologies, we performed a blind scan simulating the surgeon exploring the area to look for residuals. Fixing the probe position over the phantom disk with a random offset with respect to the phantom positions, we rotate the motorized table by a complete turn with 1 degree step angle (corresponding to 1.5 mm step along the circumference) recording a 1 s-long rate measurement at

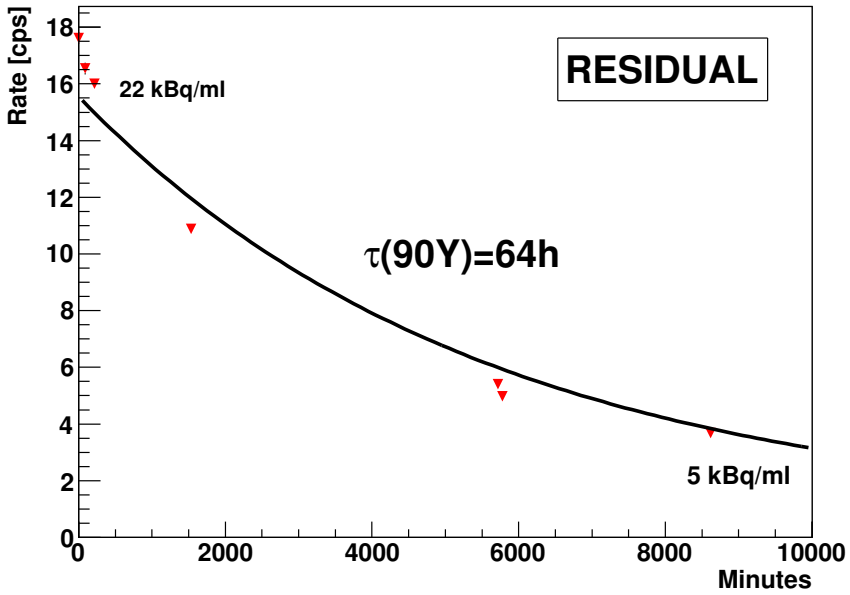

Supplementary Figure S2: **Counts-per-second observed during 1 week by the probe over the RESIDUAL phantom filled with ^{90}Y in physiological saline solution.** As expected, the rate decreases as the ^{90}Y activity. The superimposed line is the result of a fit with lifetime fixed to the one of ^{90}Y.

each step. As shown in Supplementary Fig. S3 all four phantoms were clearly detected at the 16 kBq/ml ^{90}Y activity concentration. Furthermore, the absence of a signal when the probe was located in between the samples demonstrates the insensitivity to any long-range radiation that could be produced by the activity of the phantoms.

The effect on the probe sensitivity of different phantom's footprints and of the radioactive volume thickness was also tested. As shown in Supplementary Fig. S4, moving the probe away from the phantoms results in a decrease in rate, which is halved when the centre of the probe is 0.5 mm from the edge of the sample. This is true for any phantom shape demonstrating that the depth of the sample does not affect the sensitivity of the device to the phantom's edge, making it possible to identify the real dimension of the active area.

In conclusion we verified that by administering a ^{90}Y activity similar to those used for diagnostic purposes, the probe prototype is able to identify millimetric radioactive volumes. It can detect the real dimension of the phantoms providing a fast response.

Determination of the minimal acquisition time.

Supplementary Fig. S5 shows the combination of th and t_{daq} with FP$\approx$1% and FN$<$ 5%. These curves were used, as described in the Methods section, to estimate the minimum acquisition time needed at each activity.

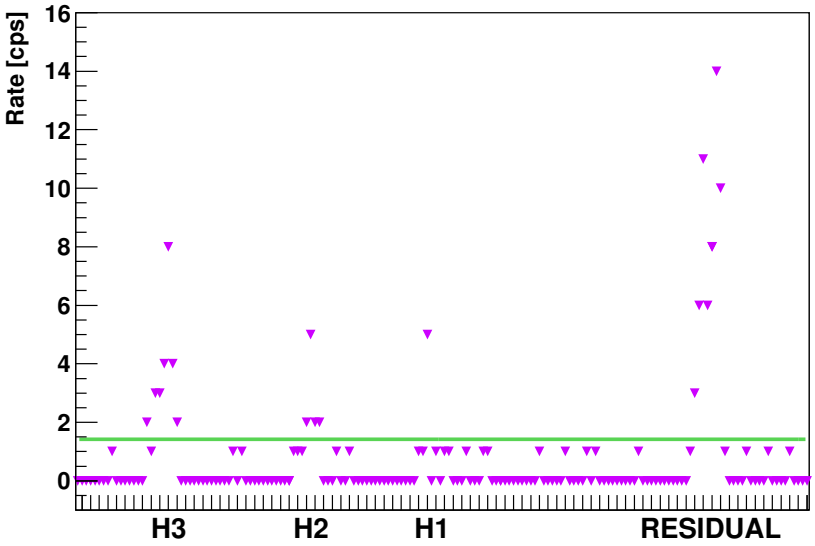

Supplementary Figure S3: **Blind scan simulating surgeon exploring the area to look for hot spots.** The counts were measured during a complete turn of the phantom disk with step of 1 degree and acquisition time of 1 s for each step. The rate increases when the probe is over a radioactive volume. Considering two counts per second sufficient to spot a residual, all samples would have been detected. The ^{90}Y activity concentration was 16 kBq/ml and the distance between the probe and the phantoms was 50 μm.

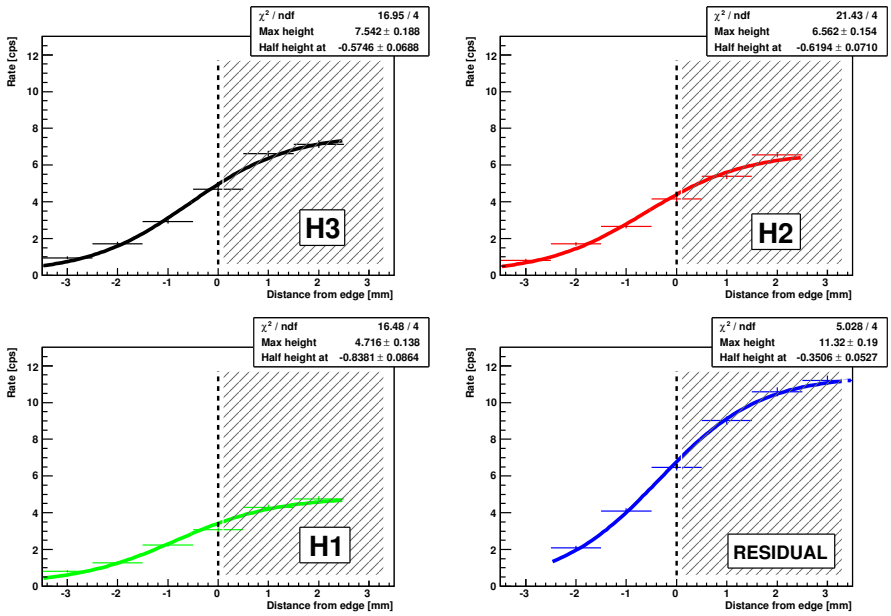

Supplementary Figure S4: **Counts-per-second measured moving the probe away from the centre of the phantoms with step of 1 mm.** In all cases the cps decreases reaching half of the central value when the probe is about 0.5 mm far from the radioactive volume edge. The ^{90}Y activity concentration was 16 kBq/ml and the distance between the probe and the phantoms was 50 μm.

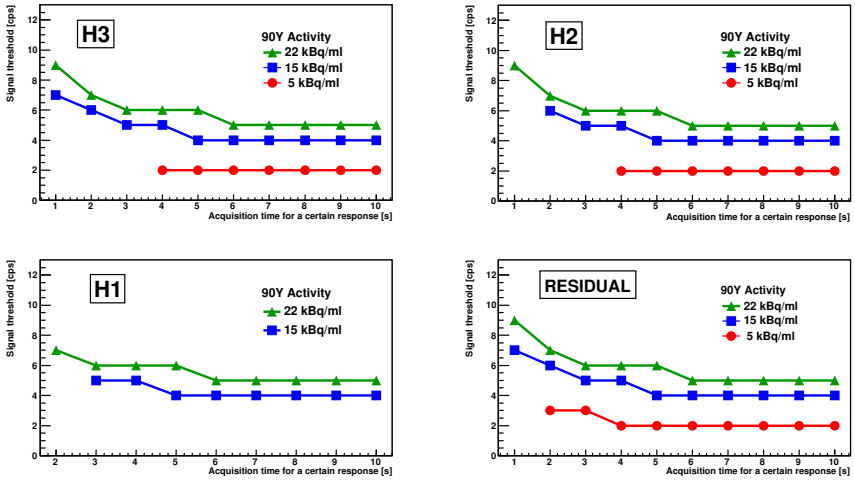

Supplementary Figure S5: **Determination of the minimal acquisition time.** As described in the Methods section, FN and FP depend on the acquisition time (t_{daq}) and the minimum signal required to claim a positive evidence (th). By requiring a false-positive probability of $\sim$1% and a false-negative probability $<$5% the allowed working points for t_{daq} and th are described. The results for the four phantoms under study are compared considering administration of radio-pharmaceutical with three different activity values. These curves were estimated in the first test medical case, the meningioma marked with ^{90}Y-DOTATOC.